Evaluation of Self-Mixing Interferometry Performance in the Measurement of Ablation Depth

Ali Gökhan Demir, Paolo Colombo, Michele Norgia, *Senior Member, IEEE*, and Barbara Previtali

***Abstract*— This paper studies self-mixing interferometry (SMI) for measuring ablation depth during laser percussion drilling of TiAlN ceramic coating. The measurement performance of SMI was investigated in a large processing range producing blind microholes with depths below and beyond the average coating thickness. Signal characteristics of the measurement system were evaluated indicating sources of disturbance. The SMI measurements were compared with a conventional measurement device based on focus variation microscopy to evaluate the measurement error. The measurement error classes were defined, as well as defining the related error sources. The results depict that the measurement error was independent of the processing condition, hence the hole geometry and ablation rate. For 76% of cases, measurement error was below the intrinsic device resolution obtainable by simple fringe counting of half a wavelength ($\lambda/2 = 0.393$ μm).**

***Index Terms*— Ceramic coating, laser ablation, laser microdrilling, laser surface texturing, process monitoring, self-mixing interferomety.**

I. Introduction

LASER ablation is a flexible micromachining process that enables high-precision noncontact machining. Due to the noncontact nature of the process, the control of machining depth is difficult. In particular, the control of machining depth on surface coatings for laser surface texturing applications becomes of paramount importance. In the case of thin ceramic surface coatings on steel substrates, high accuracy in the machining depth is required to avoid damage on coating by substrate contamination [1]. The applied coating layer is characterized by limited thickness, in the order of 2–15 μm. When the machining depth exceeds the coating thickness, the ablation conditions change drastically since the steel substrate behaves differently during the interaction with the laser beam [2]. Particularly in percussion drilling, molten steel from the substrate is deposited at the entrance of the blind hole. For laser surface texturing in view of friction applications, where a great number of microholes are realized over large areas to make a reservoir of solid or liquid lubricant [3], substrate reach can cause coating failure [2]. Thus, online monitoring capabilities are required to overcome process variations during the machining of large area components.

Several techniques for ablation depth monitoring have been proposed in the literature. Methods exploiting acoustic emission of the process [4] and mechanical vibration due to wavefront expansion [5] have been proposed. However, the majority of the techniques employ optical methods. Depending on the used method, direct or indirect measurement of the ablation depth can be made. Concerning the indirect methods, use of photodiodes (PDs) [6], [7] and optical emission spectrum [8]–[12] are the methods, which allow correlating the signal to the measured depth. In the case of optical emission spectrum, the signal can also be employed to detect change of material layer by observing the presence of a new signal component, such as plasma emission lines. Direct measurement methods commonly rely on imaging the hole itself using a probe light and a sensor. Depending on the sensor type, the measurement can be carried out in 3-D or only 1-D, hence the depth. For this purpose, Döring *et al*. [13] used a high-resolution imaging system based on charge-coupled device camera, for visualization of ablation depth in transparent materials. Interferometric methods have also been implemented to measure the ablation depth, at the end of and during the process. Papazoglou *et al*. [14] used white light interferometry implemented into the optical chain of the processing laser, which could acquire high-resolution 3-D images of the ablation area after the process. Webster *et al*. [15], [16], Leung *et al*. [17], and Ji *et al*. [18] proposed to use Fourier domain optical coherence tomography for faster acquisition of ablation depth. The technique was shown to perform with 6.2-μm depth and 100-ns time resolution. On the other hand, self-mixing interferometry (SMI) is another appealing option as a high-resolution point displacement measurement technique [19], which can be adapted in laser micromachining to monitor ablation depth [20]–[22]. The depth resolution is intrinsically high, since it is half the wavelength of the interferometer (typically $\lambda/2 < 0.5$ μm). The system also flexibly allows for increasing the temporal resolution, as megahertz level electronic bandwidths (BWs) are achievable. Previous work [23] showed that stable SMI measurements in ceramic coatings ablation were possible in the presence of a side gas jet. Although its potential use in ablation depth monitoring has been proven, the measurement performance of SMI in microdrilling depth measurement has not been studied

Manuscript received March 14, 2016; revised July 14, 2016; accepted July 15, 2016. The Associate Editor coordinating the review process was Dr. George Xiao. *(Corresponding author: Ali Gökhan Demir.)*

A. G. Demir, P. Colombo, and B. Previtali are with the Department of Mechanical Engineering, Politecnico di Milano, Milan 20156, Italy (e-mail: aligokhan.demir@polimi.it).

M. Norgia is with the Department of Electronics, Information and Bioengineering, Politecnico di Milano, Milan 20133, Italy.

Color versions of one or more of the figures in this paper are available online at http://ieeexplore.ieee.org.

Digital Object Identifier 10.1109/TIM.2016.2596038

previously. SMI has been used and characterized extensively for measurement of displacement [24], [25], distance [26], vibration [27], speed [19], and flow [28], [29] in different dimensional scales. On the other hand, ablation depth monitoring requires demanding measurement accuracy, in a scale comparable with the resolution of the device. Moreover, the ablation phenomenon itself reduces the signal quality in measurement, which adds up to the complexity of the problem. Characterization of the measurement performance is of high importance when the method should monitor depth of blind holes on coatings with limited depth (1–15 μm). Hence, the number of fringes to appear will be few, typically between 2 and 35. Errors in fringe appearance and counting can become comparable with the measured quantity.

In this paper, SMI is applied in the laser percussion drilling of TiAlN ceramic coating deposited on AISI D2 steel. The 12-μm-thick TiAlN coating was drilled with a pulsed green fiber laser, while the SMI was applied with a 785-nm laser diode (LD). In particular, the ablation depth measurement system is required to avoid incorrect measurement in proximity of coating-substrate interface. Accordingly, the measurement requirements were explained. The signal characteristics were compared with the signals obtained during the displacement of a macro target. The measurement accuracy of the employed method was evaluated by comparison with a conventional surface measurement instrument based on focus-variation microscopy.

II. Ablation Depth Monitoring System Based on Self-Mixing Interferometry

Conventional interferometry technique used for displacement measurement (Michelson interferometry) uses a reference and a measurement arm. Typically, two measurement channels are used; otherwise, the displacement direction is ambiguous. SMI exploits interference occurring in the laser cavity due to back-reflected light [19]. LDs are the most common choice for a self-mixing interferometer. A PD is usually available, mounted at the rear mirror of the laser chip, which is used to measure the power fluctuations due to the interference. As shown in Fig. 1(a), in an SMI configuration, a small portion of the emitted beam that is back reflected from a remote target enters the cavity after being attenuated in the external cavity. The reflected laser field phase depends on the distance of the reflecting body at a given time instance [19]. In SMI, the back-reflected field E_r adds to the lasing field E_l, modulating its amplitude and frequency. The interferometric phase can be retrieved from the change of the optical power measured. The periodic function of the interferometric phase, hence the signal shape, depends on the feedback parameter (C). Feedback parameter depends on the LD design and characteristics, as well as optical attenuation in the external cavity. An increase in the optical attenuation results in the decrease in the feedback parameter, hence change of the signal shape. In very weak feedback regime ($C \ll 1$), the self-mixing signal shows a cosine function shape, which results in the ambiguity of the displacement direction. In weak feedback regime ($0.1 < C < 1$), the signal shape gets distorted and has a

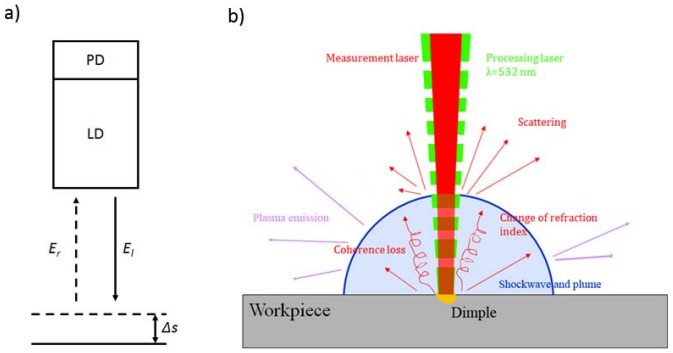

Fig. 1. (a) Working principle of SMI for displacement measurement. (b) Schematic of the optical changes around the surface due to ablation products, which are likely to disturb SMI measurements.

nonsymmetrical shape. For stable interferometric displacement measurements that are nonambiguous in direction, the feedback parameter is typically required to be at the moderate regime ($1 < C < 4.6$). Further increase in feedback parameter ($C > 4.6$) results in entering the strong feedback regime, where multiple switchings per period may occur, and the measurement is affected by an error. Working in moderate feedback regime, at each displacement of half laser wavelength ($\lambda/2$), a fringe forms. The resultant signal shows a saw-tooth shape. By fringe counting, the total displacement (Δs) is calculated as

$$\Delta s = n_{\text{frg}} \cdot \lambda/2 \tag{1}$$

where n_{frg} represents the number of fringes. The saw-tooth signal shape of SMI also provides the displacement direction.

During the laser-material interaction with nanosecond pulses, the pulse duration is long enough to generate thermal interaction that will generate vapor and molten phases of the material. In the initial phase of this interaction, plasma can also form from the material vapor. The pressure exerted on the molten phase by the vapor and plasma can cause material ejection [30]. One of the main concerns regarding the feasibility of the SMI for ablation measurements is related to these physical changes modifying the optical properties in the space close to the hole, as the measurement beam should pass through turbid media [31]. As depicted in Fig. 1(b), the measurement beam encounters the ablation products, namely, plasma, shockwave and plume, which may scatter the beam and generate coherence loss. These factors can alter the optical feedback parameter, and eventually the measurement signal can be lost. Moreover, the machined area differs from the initial surface in terms of both reflectivity and geometry. Speckle formation is also expected due to the changes in the surface morphology [32]. The use of side gas has been found to overcome the problems related to plume generation [23]. On the other hand, speckle effects are intrinsically difficult to tackle due to the fact that the measurement beam should pass through the realized hole as it is formed.

The SMI used in this paper was realized using off-the-shelf components. The design criteria are explained in detail in [23]. A GaAlAs LD with a multiquantum well structure (HL7851G from Hitachi, Ibaraki, Japan) was used as the light source. Emission wavelength of the interferometer was 785 nm. The

TABLE I
MAIN CHARACTERISTICS OF THE PROCESSING AND MEASUREMENT LASERS

Parameter	Processing	Measurement
Emission wavelength, λ	532 nm	785 nm
Emission type	Pulsed wave	Continuous wave
Output power, P	6 W (Average)	0.015 W
Pulse duration, τ	1.2 ns	n/a
Pulse repetition rate, PRR	20-300 kHz	n/a
Maximum pulse energy, E_{max}	20 µJ	n/a
Beam quality factor, M^2	1.1	1.2
Collimated beam diameter	3.49 mm	2.9 mm (fast axis) 5.1 mm (slow axis)
Focused beam diameter (f=100 mm), d_0	21.7 µm	41.4 µm (fast axis) 23.5 µm (slow axis)

depth measurement resolution obtainable by simple fringe counting is half wavelength, and at stable conditions, it is equal to 392.5 nm, which might drift ±2 nm due to temperature and current variations. The monitor PD current was converted by a single-stage transimpedance amplifier, realized by a transimpedance amplifier (OPA380 from Texas Instruments, Dallas, TX, USA) with gain equal to 420 kΩ. In these conditions, the BW of the interferometer was about 1 MHz, allowing us to capture the fast ablation phenomenon and obtain signals with good signal-to-noise ratio. The SMI signal was acquired with a digital oscilloscope characterized by 350-MHz maximum BW, 5-GS/s sampling rate, and $16 \cdot 10^6$ record length (TDS5034B from Tektronix, Oregon, USA).

The used processing laser was a master oscillator power amplifier fiber laser operating with green wavelength (YLPG-5 from IPG Photonics, Oxford, MA, USA). The measured average and estimated maximum peak powers are 6 W and 16 kW, respectively. The processing laser is characterized by a delay and ramped emission in the initial phase of the emission [23]. In order to control the number of pulses emitted, the emission delay was measured for all experimented conditions and was added to the effective drilling time for piloting the laser with the correct modulation duration. In the following graphs, the drilling time after the emission delay is exhibited. The processing beam was combined with the beam of the self-mixing interferometer with a dichroic mirror (DMLP567 from Thorlabs, Newton, NJ, USA). The beams were focused using an achromatic lens with 100-mm focal length (AC254-100-A-ML from Thorlabs) and launched onto the workpiece on the same point (see Fig. 2). The main specifications of the processing and measurement lasers are summarized in Table I.

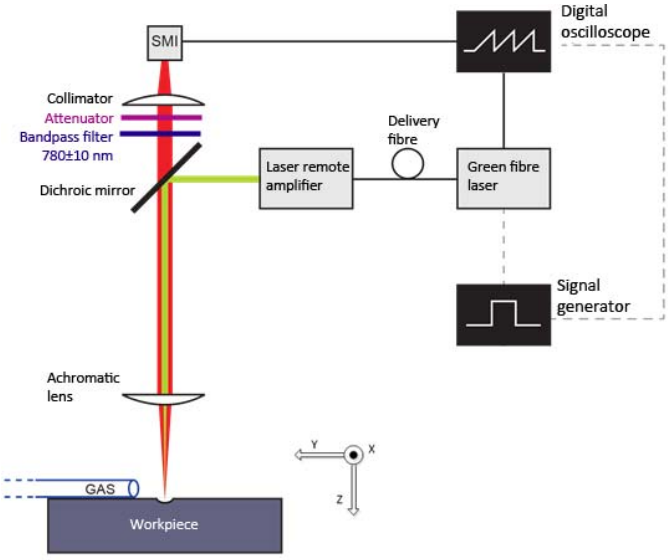

Fig. 2. Ablation monitoring setup consisting of the processing laser and self-mixing interferometer.

III. PERFORMANCE OF THE SELF-MIXING INTERFEROMETER

The monitoring system was evaluated during the percussion microdrilling of TiAlN ceramic coating deposited on AISI D2 tool steel (Balinit Lumena from Oerlikon Balzers, Balzers, Liechtenstein). The coating thickness was measured as 12.1 ± 0.7 μm. Measured average surface roughness was 0.15 ± 0.02 μm. Laser percussion microdrilling was the used processing strategy, which is the basis of point-by-point laser surface texturing. In particular, for its application in laser ablation, the measurement error should not depend on the ablation depth, hence the laser ablation conditions. Moreover, the SMI system should be able to reveal ablation depth change with error margin lower than the variability of the coating thickness.

Therefore, the performance measurement of the SMI system was evaluated in laser microdrilling conditions generating hole depths below and beyond the coating thickness. The system is required to perform well independently of the processing conditions, and hence, the whole feasibility range producing hole depths between 1 and 13 μm was explored. In this way, similar hole depths could be obtained using different laser process conditions. In order to evaluate the depth increase as a function of the laser parameters, four levels of pulse energy (E), five levels of number of pulses (N), and two levels of pulse repetition rate (PRR) were selected (see Table II). Experiments were applied using N_2 side gas jet at 1 bar to avoid signal loss due to ablation plume. All experimental conditions were repeated five times. Hole depth was measured offline, from the acquired SMI signals through manual fringe counting (h_{SMI}). The accuracy of the SMI measurements was determined in comparison with a conventional surface

TABLE II

EXPERIMENTAL PLAN FOR ACCURACY EVALUATION OF THE MEASUREMENT SYSTEM

Fixed parameters		
Focal position	h_f [mm]	0
Varied parameters		
Pulse energy	E [μJ]	5, 10, 15, 20
Number of pulses	N [-]	50, 100, 150, 200, 250
Pulse repetition rate	PRR [kHz]	160, 300
Measured variable		
Hole depth measured with SMI	h_{SMI} [μm]	
Hole depth measured with FVM	h_{FVM} [μm]	

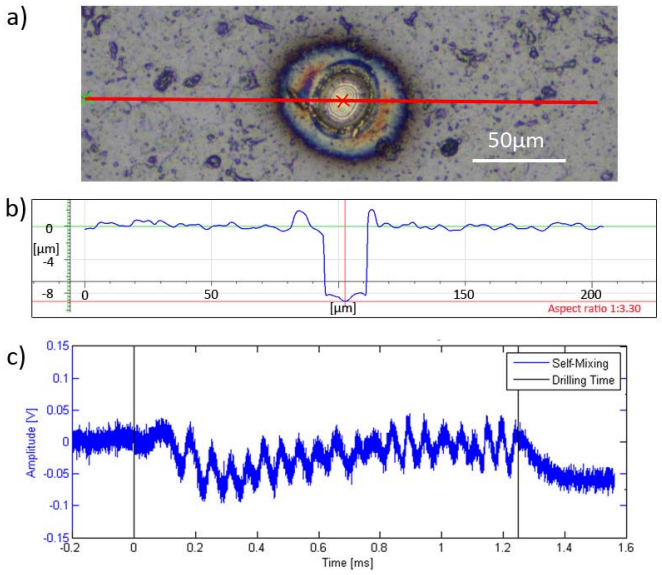

Fig. 3. Determination of hole depth with FVM and SMI ($E = 10$ μJ, PRR = 160 kHz, and $N = 200$). (a) Real color image acquired by FVM depicting the position of the depth profile. (b) Corresponding depth profile. (c) SMI signal belonging to the hole.

geometry measurement device (InfiniteFocus from Alicona, Graz, Austria) based on focus variation microscopy (FVM). 3-D image of each hole was acquired using 50X magnification lens. In this configuration, vertical and horizontal resolutions were 12 nm and 1 μm, respectively. The hole depth (h_{FVM}) was determined as the distance of the lowest point of the acquired hole with respect to the surface, as shown in Fig. 3. Fig. 3(c) shows the self-mixing signal acquired during the ablation procedure: the fringes are clearly measurable and indicate a continuous growth of the hole during the drilling time.

Depth measurements were compared pairwise on each single hole, defining the measurement error (e) of SMI as

$$e = h_{SMI} - h_{FVM}. \quad (2)$$

The repeatability of the FVM device used for measurement comparison was also analyzed by designed experiments. Three conditions (K) representing low (average $h_{FVM} = 2.99$ μm), medium (average $h_{FVM} = 6.39$ μ m), and high (average $h_{FVM} = 12.07$ μm) hole depths were chosen. The chosen holes were acquired with the FVM five times. Each acquisition

TABLE III

ANOVA TABLE FOR HOLE DEPTH MEASURED BY FOCUS VARIATION MICROSCOPE h_{FVM} (μm). *DF*: DEGREES OF FREEDOM; *F-VALUE*: THE TEST STATISTIC USED TO DETERMINE WHETHER THE TERM IS ASSOCIATED WITH THE RESPONSE; *P-VALUE*: A PROBABILITY THAT MEASURES THE EVIDENCE AGAINST STATISTICAL SIGNIFICANCE; *S*: STANDARD DEVIATION OF HOW FAR THE DATA VALUES FALL FROM THE FITTED VALUES; R^2: PERCENTAGE OF VARIATION IN THE RESPONSE THAT IS EXPLAINED BY THE MODEL; AND R^2_{adj}: THE VALUE OF R^2 ADJUSTED FOR THE NUMBER OF PREDICTORS IN THE MODEL RELATIVE TO THE NUMBER OF OBSERVATIONS

Source	DF	F-Value	P-Value
Condition (K)	2	86630.89	0
Acquisition repetition (AR)	4	1.06	0.391
Measurement repetition (MR)	4	2.09	0.105
K*AR	8	1.93	0.089
K*MR	8	0.45	0.880
AR*MR	16	1.00	0.48
Error	32		
Total	74		
S=0.078	R^2=99.98%	R^2_{adj}=99.96%	

was also measured five times. All the acquisitions and measurements were carried out in random order. The resultant experimental plan was composed of condition (K) with three levels, acquisition repetition (AR) with five levels, and measurement repetition (MR) with five levels as the investigated factors. Analysis of variance (ANOVA) was applied on the measurement results. Bonferroni criteria were applied to test the statistical significance of the parameters and their interaction. The overall level of statistical significance family error (α_{FAM}) was set at 5%. Accordingly, statistical significance level for each parameter and interaction was calculated as α_{FAM}/g, where g is the total number of statistical tests in ANOVA. For statistical significance, the p-value associated with a parameter or interaction has to be smaller than this calculated value [33]. Table III reports the results of ANOVA. With three parameters and three second-order interactions, the statistical significance for each test is 0.83%. It can be observed that the only significant parameter over the measured depth is condition (K), hence the measured hole depth itself (p-value $< 0.83\%$). The AR and MR and their interactions do not significantly alter the outcome of the measurement. In particular, the standard deviation pooled over different ARs and MRs were 45, 99, and 92 nm for low, medium, and high hole depths, respectively. Such values are well below the resolution of the SMI employing fringe counting used in the experimentation, rendering FVM a suitable device for the performance evaluation of SMI.

IV. RESULTS

A. Self-Mixing Interferometry Signal Characteristics

Fig. 4 compares the SMI signals obtained during stable and disturbed conditions. The signal shown in Fig. 4(a) represents the conventional SMI signal in moderate feedback regime obtained during the displacement of a metallic target.

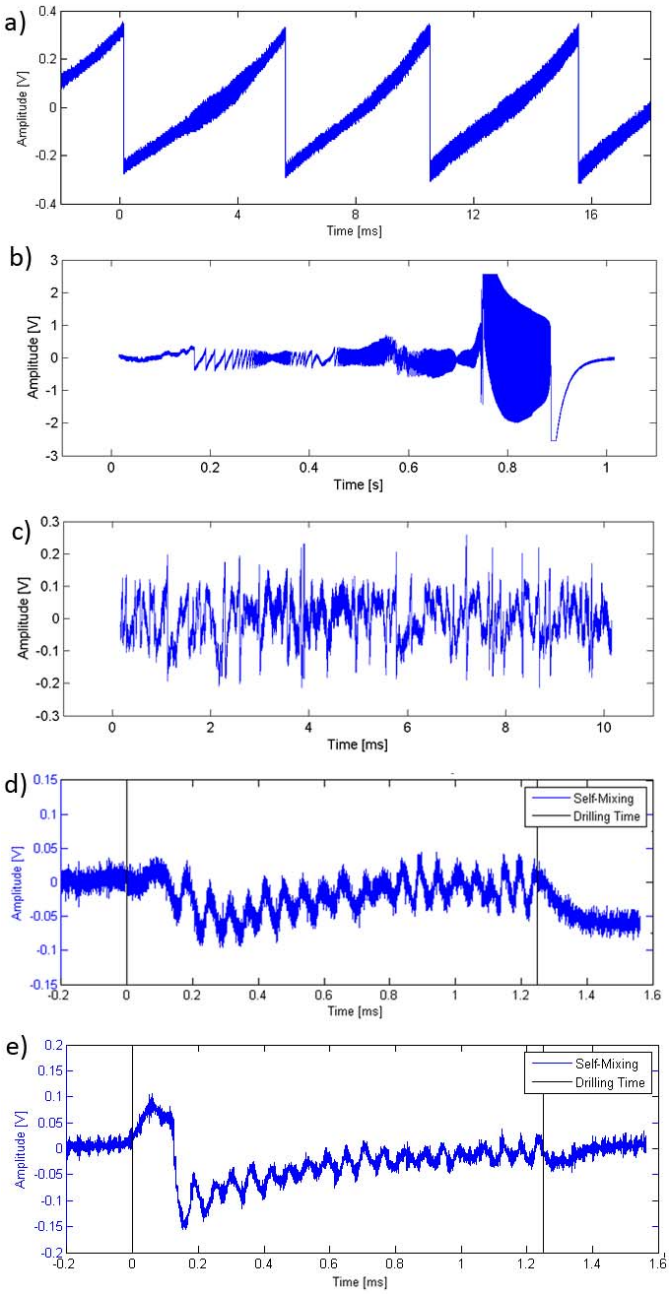

Fig. 4. SMI signals representing stable and disturbed measurement conditions. (a) During the displacement of a metallic target. (b) Mode hopping caused by excessive back reflection from the remote target. (c) Without target displacement in the presence of He flow. (d) Easy readout signal type during microdrilling of TiAlN coating ($E = 10$ μJ, PRR $= 160$ kHz, and $N = 200$). (e) Difficult readout signal type ($E = 10$ μJ, PRR $= 160$ kHz, and $N = 200$).

The signal shows high amplitude (500-mV peak-to-peak fringe amplitude), and the saw-tooth shape is well defined. One of the important issues related to measurement stability is the mode hopping phenomenon. In mode hopping, the emission wavelength of the diode laser changes making discrete jumps, since the laser switches from one longitudinal mode to another [34]. Mode hopping is caused by laser case temperature, injection current, and optical feedback. Both case temperature and injection current were kept stable during the experiments. However, the optical feedback was variable since the ablation phenomenon also changes the optical properties of the material surface during the process [35], [36]. The material reflectivity and surface curvature are both varied throughout the process. Moreover, within this measurement scheme, the SMI is focused to a small spot increasing the intensity on a small area. Due to the low surface roughness of the material and at normal incidence, such as the one presented in this paper, the reflected light amount is expected to be higher and scattering is expected to be lower compared with rough and diffusive surfaces [37]. Hence, the amount of back reflected light may be excessive during the operation, causing the system to operate in the so-called strong feedback regime ($C > 4.6$). In this regime, SMI measurements are not always possible. Due to all these factors, the system is also prone to mode hopping. Fig. 4(b) demonstrates mode hopping phenomenon occurred during the placement of the workpiece. Mode hopping requires careful adjustment of the diaphragm in the optical chain to avoid entering in strong feedback regime, but also allowing enough optical feedback to work in moderate feedback regimes.

Another issue is related to the used process gas in the laser microdrilling process. As a matter of fact, an interferometer will measure the change in optical path difference, which can be induced by a change in distance, in refractive index or both [38]. Refractive index of air is 1.0002751 at 785-nm wavelength [39]. For the same wavelength, the refractive index of N_2 is reasonably close to air being 1.0002963, since this gas corresponds to the major component in air [40]. On the other hand, the refractive index of He is 1.00003481, which is much smaller [41]. Hence, the He flow under the SMI generates fringes due to refractive index variation without any target displacement as shown in Fig. 4(c). Accordingly, the method is not suitable, if a process gas with refractive index very different from the ambient atmosphere is blown over the measurement area.

On the other hand, the SMI signals acquired during the laser microdrilling process are remarkably different from the signals obtained in conventional displacement measurement conditions. The signals shown in Fig. 4(d) and (e) represent SMI signals obtained during ablation process. It can be observed that the faster edge of the saw-tooth shape is less steep. The peak-to-peak fringe amplitude in this case is around 50 mV. The present fringe amplitude during laser ablation is about five times higher compared with [23], where higher BW (35 kHz) was employed. The results demonstrate that 1-MHz BW level is more suitable as dynamic features of the signal are not compromised with higher signal-to-noise ratio. Therefore, the feedback parameter is decreased; however, the operation is still in moderate feedback regime. Due to the previously described changes in optical properties of the machined surface, the amount of reflected light can reduce, which also reduces the feedback parameter. Another common feature of the SMI signals in ablation monitoring is the ascending or descending slopes around the signal average value. This characteristic is attributed to the speckle phenomenon present in the so-called noncooperating targets [32]. In conventional SMI measurements, signal average shifts from zero due to

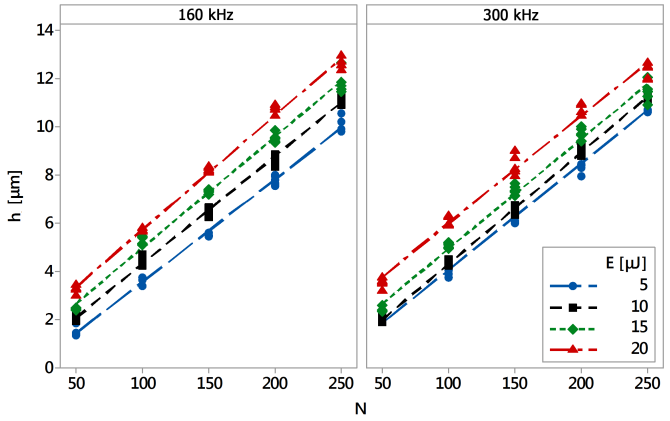

Fig. 5. Hole depth (h) as a function of process parameters pulse energy (E), number of pulses (N), and PRR measured by FVM.

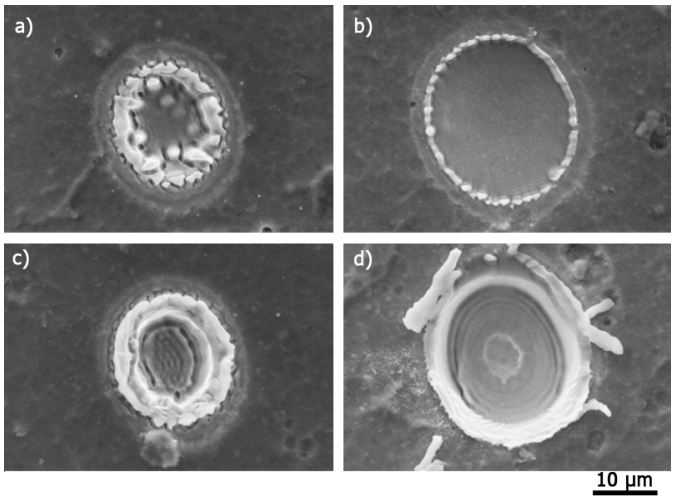

Fig. 6. Comparison of hole morphology obtained with different laser microdrilling parameters, showing similar depth and diameter conditions. (a) $E = 5$ μJ, PRR $= 160$ kHz, and $N = 100$. (b) $E = 20$ μJ, PRR $= 300$ kHz, and $N = 50$. (c) $E = 5$ μJ, PRR $= 160$ kHz, and $N = 250$. (d) $E = 20$ μJ, PRR $= 300$ kHz, and $N = 200$.

target surface scanning [see Fig. 4(e)]. The scattered light causes speckle formation. Consequently, signal fading and deformation, as well as fringe amplitude variation occur. During the laser microdrilling operation, the target changes the surface geometry, and hence speckle formation is inevitable. The presence of these defects renders automated fringe counting difficult and in some cases impossible. Signal correction to overcome speckle effects is evidently vital for this purpose. Automated fringe counting and moreover signal analysis for retrieving the displacement within incomplete fringes should be considered, together with elaboration algorithm working in the frequency domain [42].

Another important feature of the SMI signals during the laser microdrilling process is related to the delay in the occurrence of the first fringe. This is expected to be due to the ramped emission profile in the initial part of the pulse train, which generates a reduced ablation rate. Hence, SMI is capable of measuring the changes in the ablation rate even within the displacement of a single fringe.

During ablation monitoring, these defects were present. A primary distinction was carried out for the readability of the signals as easy and difficult. The SMI signal shown in Fig. 4(d) depicts an easy readout as signal deformation due to reduced feedback parameter and speckle is limited. On the other hand, the SMI signal in Fig. 4(e) is an example for difficult readout due to a marked speckle effect and variable signal shape due to changing feedback parameter. The occurrence of difficult readout signals was high, consisting of 55% of the 199 acquired signals. In the analysis, all signals were used for fringe counting; however, the effect of signal quality on the error was also evaluated.

B. Evaluation of Measurement Error

Fig. 5 reports the hole depth measurements obtained by FVM, over the experimented region as a function of process parameters. It can be observed that within the experimented region, hole depths could vary between 1.5 and 13 μm. Both pulse energy and number of pulses were effective in increasing hole depth, whereas the influence of PRR was limited. Fig. 6 compares the hole geometries obtained with different process parameter combinations. The holes exhibit slight ellipticity, which can be only partially attributed to the processing laser beam shape. The geometrical imperfection components of the used experimental optical system and their alignment are also expected to contribute. It can also be observed that the bottom of the blind holes show a significantly different roughness profile compared with the nonmachined surface. Such a roughness profile change can cause change in the reflectivity of the material at the bottom of the hole, hence reduce the optical feedback. Moreover, roughness profile induces a variable surface profile at the bottom of the hole, which can alter the measured displacement. However, this second contribution is expected to be much less significant being in a smaller dimensional range compared with the resolution obtained by fringe counting. The impact of roughness can be more relevant with improved resolution of the device through signal processing. The images show that holes with similar depth could be achieved with different diameters and vice versa. In particular, the holes shown in Fig. 6(a) and (b) are characterized by a similar low depth (average $h_{\mathrm{FVM}} = 3.38$ μm), whereas the ones in Fig. 6(c) and (d) exhibit high depth (average $h_{\mathrm{FVM}} = 10.38$ μm). On the other hand, the holes in Fig. 6(a) and (c) show a similar small diameter (average $D = 18$ μm), whereas Fig. 6(b) and (d) shows holes with similar and larger diameters (average $D = 24$ μm). Accordingly, within the experimental campaign, the effect of the hole diameter is included.

Fig. 7(a)–(d) exhibits SMI signals of obtained in increasing number of pulses with fixed pulse energy and PRR levels. Fig. 7(a)–(d) clearly depicts that the number of fringes increases with the number of pulses, following the same trend observed with the FVM measurements. Fig. 7(e) shows the hole depth measured by SMI employing simple fringe counting. It can be observed that the results are very close to the measurements obtained by FVM and maintain the same linear increase as a function of number of pulses (N) and

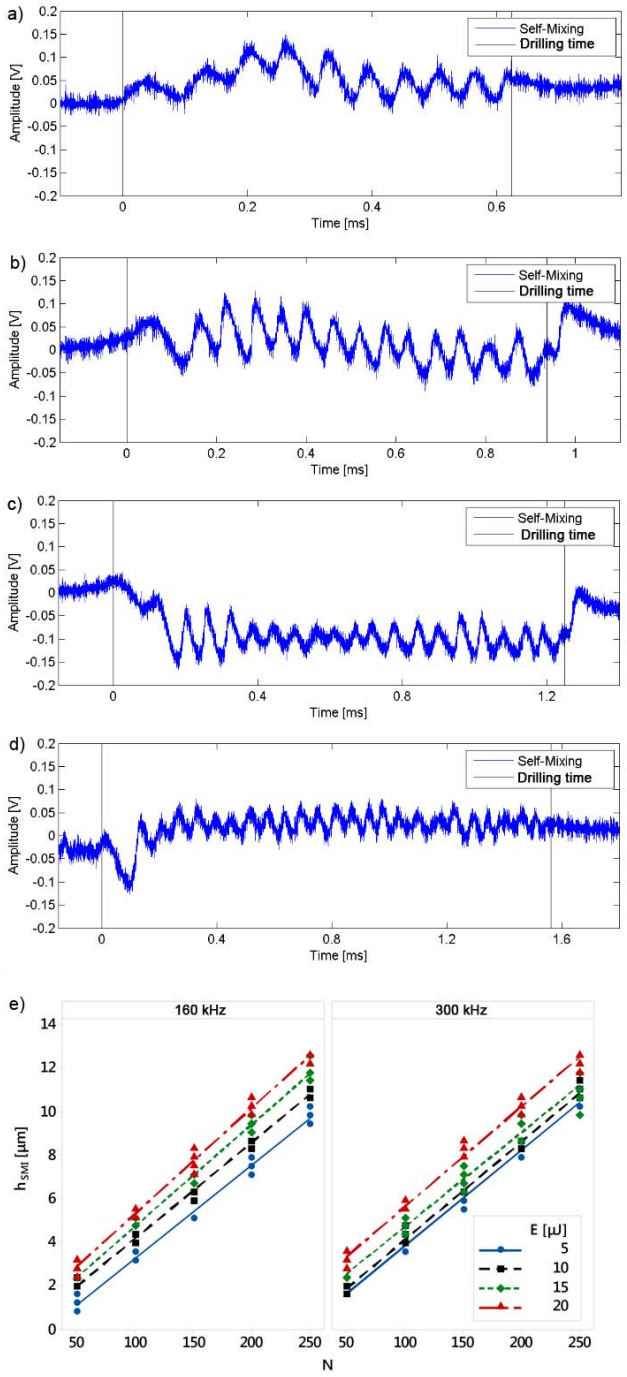

Fig. 7. SMI signal examples during the ablation of holes with different depths. Laser microdrilling parameters were $E = 10$ μJ and PRR $= 160$ kHz with variable number of pulses N. (a) $N = 100$, $n_{frg} = 10$, and $h_{SMI} = 3.93$ μm. (b) $N = 150$, $n_{frg} = 16$, and $h_{SMI} = 6.28$ μm. (c) $N = 200$, $n_{frg} = 22$, and $h_{SMI} = 8.64$ μm. (d) $N = 250$, $n_{frg} = 28$, and $h_{SMI} = 10.21$ μm. (e) Hole depth (h) as a function of process parameters pulse energy (E), number of pulses (N), and PRR measured by SMI.

pulse energy (E), whereas no significant effect of PRR is visible.

Over the total number of 200 experiments resulting from 40 experimental conditions and five replications for each, only one was not included in the further qualitative and statistical analyses due to experimental error. Each microhole realized experimented condition was measured with FVM, and the acquired SMI was used to measure the depth of the same hole. In Fig. 8(a), the error of SMI measurements is shown as a function of the process parameters and signal quality classification. The error classes are also highlighted as missing or excess fringe counts with the dashed lines. Fig. 8(b) shows these error classes in their corresponding occurrence percentage. The main results coming from the analysis can be listed as follows.

TABLE IV

ANOVA TABLE FOR MEASUREMENT ERROR e (μm). *DF*: DEGREES OF FREEDOM; *F-VALUE*: THE TEST STATISTIC USED TO DETERMINE WHETHER THE TERM IS ASSOCIATED WITH THE RESPONSE; *P-VALUE*: A PROBABILITY THAT MEASURES THE EVIDENCE AGAINST STATISTICAL SIGNIFICANCE; S: STANDARD DEVIATION OF HOW FAR THE DATA VALUES FALL FROM THE FITTED VALUES; R^2: PERCENTAGE OF VARIATION IN THE RESPONSE THAT IS EXPLAINED BY THE MODEL; AND R^2_{adj}: THE VALUE OF R^2 ADJUSTED FOR THE NUMBER OF PREDICTORS IN THE MODEL RELATIVE TO THE NUMBER OF OBSERVATIONS

Source	DF	F-Value	P-Value
E [µJ]	3	1.74	0.161
PRR [kHz]	1	1.08	0.301
N	4	0.9	0.456
E [µJ]*PRR [kHz]	3	1.48	0.221
E [µJ]*N	12	2.26	0.011
PRR [kHz]*N	4	1.53	0.201
E [µJ]*PRR [kHz]*N	12	1.08	0.38
Error	157		
Total	196		
S=0.236	R^2=28.07%	R^2_{adj}=10.20%	

1) *SMI Signal Quality Is Adequate to Avoid Misreading in General:* The SMI measurements are clustered around same values within the same processing conditions. This is due to the discrete incremental steps in the measurement based on fringe counting and the fact that all the measurements are multiples of $\lambda/2$. As shown in Fig. 8(a), the overall results show that the error is confined between 0 and $-\lambda = -0.785$ μm. As a matter of fact, all error values falling below this range (between $-\lambda$ and -2λ) correspond to signals with difficult readout.
2) *The Measurement Error Is Independent of the Processing Conditions:* As depicted in Fig. 8(a), the measurement error does not follow a certain trend across the experimental range. The dependence of error on the processing conditions was evaluated with ANOVA. Bonferroni criteria were applied with $\alpha_{FAM} = 5\%$. With three parameters, three second-order interactions, and one third-order interaction, the statistical significance for each test is 0.71%. As depicted in Table IV, none of the parameters was found to be significant. This result confirms that the SMI measurement is not affected by the hole geometry, particularly by diameter or depth. The measurement campaign shows that the same depth can be obtained in different time durations, using lower

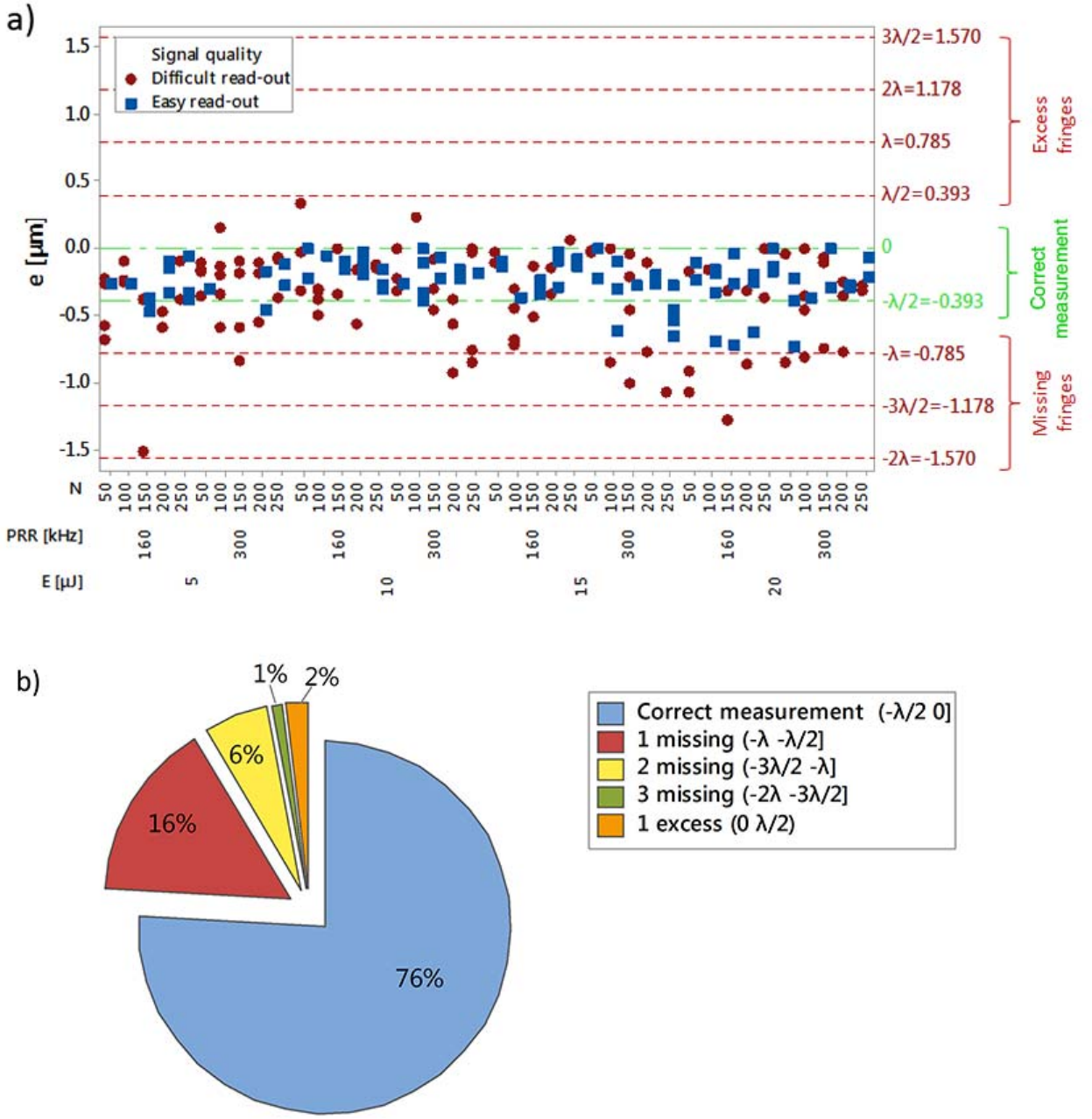

Fig. 8. (a) Measurement error as a function of process parameters and signal quality. The dashed lines indicate the error classes as a function of fringe count. (b) Occurrence percentage of the error classes. The percentages refer to 199 total number of measurements.

or higher PRRs. Therefore, it can be concluded that the error does not depend on the depth increase rate as well.

3) *Measurement Error Margin Is Lower Than the Variability of the Coating Thickness:* The majority of the measurement error (76% of the whole experimented range) falls between zero and one missing fringe range (between 0 and $-\lambda/2$). This range represents the capability of the device, since the error is lower than the resolution obtained by fringe counting ($\lambda/2 = 0.393$ nm). Hence, in the majority of the cases, the SMI error is acceptable for the application. Only in 6% of the experimented range (11 measurements), the error corresponds to more than one missing fringe (between $-\lambda$ and -2λ), which is larger than the thickness variation. The device is capable of measuring with adequate error margin in the most critical region, the coating/substrate interface.

4) *SMI Measurements Underestimate the Hole Depth:* In Fig. 8(a), it can be observed that the error is accumulated around negative values, which depicts that the SMI system tends to underestimate the hole depth. This phenomenon is due to the functioning principle of SMI. A fringe will form when the displacement is increased by $\lambda/2$. When, the displacement ends without reaching a multiple of $\lambda/2$, the remaining part will generate an incomplete fringe. Such an increment is not captured in fringe counting, but can be estimated by signal

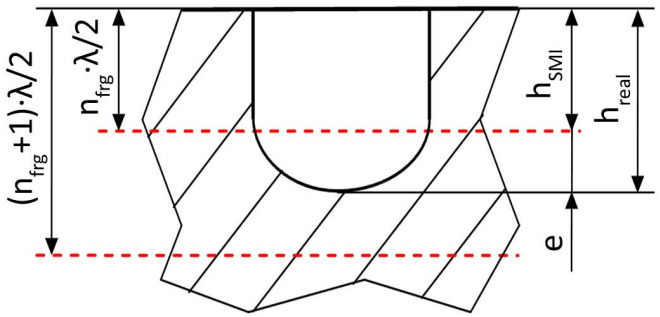

Fig. 9. Schematic of the error underestimation due to incomplete fringes.

processing. As shown in Fig. 9, during the microdrilling process, the hole depths that fall between two discrete fringe numbers will be measured with a smaller depth compared with the real one. Due to this reason, only the region between $-\lambda/2$ and 0 can be considered as correct measurements within the capability of the device. Regarding other error classes, the positive error obtained in region between 0 and $\lambda/2$ is due to signal errors. The range between $-\lambda/2$ and $-\lambda$ corresponds to one missing fringe and is acceptable for measurements based on manual fringe counting. Finally, in the region between $-\lambda$ and -2λ, error classes of 2 and 3 missing fringes exist. In these error classes, the signal quality was always found to be low, which is the main cause for the error.

V. Conclusion

In this paper, the use of SMI for ablation depth monitoring of TiAlN ceramic coating was demonstrated. For the first time, the measurement accuracy of SMI for ablation depth monitoring was methodologically investigated in a large processing range. In particular, the performance of the measurement method was evaluated regarding the process requirements. For this purpose, the signal characteristics of SMI measurement system were investigated. It was observed that the SMI measurements was sensitive to increased optical feedback due to tightly focused beam and refractive index changes that may occur due to the used side gas jet. Moreover, the SMI signals suffered from changes in reflectivity and speckle formation during ablation, which significantly reduce the signal quality in comparison with signals obtained in conventional applications. The measurement error of SMI was found to be below resolution obtainable by simple fringe counting ($\lambda/2 = 0.393$ μm) for the larger part of the experimental range (76%). Overall, the error did not exceed $2\lambda = 1.57$ μm. The SMI measurements were also found to underestimate the hole depth due to incomplete fringe formation.

Under the light of the obtained results, it can be concluded that the SMI measurement system is capable of measuring the ablation depth, with an error margin below the coating thickness variation. Moreover, the results show that further reduction of measurement error is possible through improving the signal quality. Improvement of the signal quality during the measurement is limited due to the complicated nature of the ablation process, through which the drilled microhole acts as a noncooperating target. A more feasible way for improved measurement performance appears to be in the postprocessing stage. The complexity of the postprocessing strategies, however, would increase the computation time and render eventually the online use of this monitoring method more difficult. Accordingly, the acceptable error margin should be considered for the given application. Increasing the device resolution by reducing the wavelength is another possibility for reducing error margin. It should be noted that the chosen wavelength should not coincide with the plasma luminescence of the workpiece material to avoid its integration to the PD, and the electronic BW should be matched to acquire the higher number of fringes observed in the same drilling time.

Acknowledgment

The authors would like to thank Prof. Q. Semeraro for the valuable discussion and support in data analysis phase. They would also like to thank IPG Italy for providing the green fiber laser source.

References

[1] A. G. Demir, N. Lecis, B. Previtali, and D. Ugues, "Scratch resistance of fibre laser surface textured TiN coatings," *Surf. Eng.*, vol. 29, no. 9, pp. 654–659, Oct. 2013.

[2] A. G. Demir, K. Pangovski, W. O'Neill, and B. Previtali, "Laser micromachining of TiN coatings with variable pulse durations and shapes in ns regime," *Surf. Coat. Technol.*, vol. 258, pp. 240–248, Nov. 2015.

[3] L. Vandoni, A. G. Demir, B. Previtali, N. Lecis, and D. Ugues, "Wear behavior of fiber laser textured TiN coatings in a heavy loaded sliding regime," *Materials*, vol. 5, no. 11, pp. 2360–2382, Nov. 2012.

[4] T. Kurita, T. Ono, and T. Nakai, "A study of processed area monitoring using the strength of YAG laser processing sound," *J. Mater. Process. Technol.*, vol. 112, pp. 37–42, May 2001.

[5] M. Stafe, C. Negutu, and I. M. Popescu, "Real-time determination and control of the laser-drilled holes depth," *Shock Waves*, vol. 14, nos. 1–2, pp. 123–126, Jun. 2005.

[6] D. P. Hand, C. Peters, F. M. Haran, and J. D. C. Jones, "A fibre-optic-based sensor for optimization and evaluation of the laser percussion drilling process," *Meas. Sci. Technol.*, vol. 8, pp. 587–592, Jun. 1997.

[7] A. Stournaras, K. Salonitis, and G. Chryssolouris, "Optical emissions for monitoring of the percussion laser drilling process," *Int. J. Adv. Manuf. Technol.*, vol. 46, nos. 5–8, pp. 589–603, Jan. 2010.

[8] V. Kanicky, J. Musil, and J.-M. Mermet, "Determination of Zr and Ti in 3-μm-thick ZrTiN ceramic coating using laser ablation inductively coupled plasma atomic emission spectrometry," *Appl. Spectrosc.*, vol. 51, no. 7, pp. 1037–1041, Jul. 1997.

[9] F. Le Guern *et al.*, "Co-deposited layer characterisation and removal control by optical emission spectroscopy coupled to nano-second laser ablation," *Fusion Eng. Des.*, vol. 81, pp. 1503–1509, Feb. 2006.

[10] H. Balzer, M. Hoehne, V. Sturm, and R. Noll, "Online coating thickness measurement and depth profiling of zinc coated sheet steel by laser-induced breakdown spectroscopy," *Spectrochim. Acta B, Atom. Spectrosc.*, vol. 60, pp. 1172–1178, Aug. 2005.

[11] C. Grisolia *et al.*, "*In-situ* tokamak laser applications for detritiation and co-deposited layers studies," *J. Nucl. Mater.*, vols. 363–365, pp. 1138–1147, Jun. 2007.

[12] J. Ruiz, A. González, L. M. Cabalín, and J. J. Laserna, "On-line laser-induced breakdown spectroscopy determination of magnesium coating thickness on electrolytically galvanized steel in motion," *Appl. Spectrosc.*, vol. 64, no. 12, pp. 1342–1349, Dec. 2010.

[13] S. Döring, S. Richter, S. Nolte, and A. Tünnermann, "*In situ* imaging of hole shape evolution in ultrashort pulse laser drilling," *Opt. Exp.*, vol. 18, no. 19, pp. 20395–20400, Sep. 2010.

[14] D. G. Papazoglou, V. Papadakis, and D. Anglos, "*In situ* interferometric depth and topography monitoring in LIBS elemental profiling of multilayer structures," *J. Anal. Atom. Spectrom.*, vol. 19, no. 4, pp. 483–488, 2004.

[15] P. J. L. Webster, J. X. Z. Yu, B. Y. C. Leung, M. D. Anderson, V. X. D. Yang, and J. M. Fraser, "*In situ* 24 kHz coherent imaging of morphology change in laser percussion drilling," *Opt. Exp.*, vol. 35, no. 5, pp. 646–648, Mar. 2010.

[16] P. J. L. Webster, L. G. Wright, K. D. Mortimer, B. Y. Leung, J. X. Z. Yu, and J. M. Fraser, "Automatic real-time guidance of laser machining with inline coherent imaging," *J. Laser Appl.*, vol. 23, no. 2, p. 022001, May 2011.

[17] B. Y. C. Leung, P. J. L. Webster, J. M. Fraser, and V. X. D. Yang, "Real-time guidance of thermal and ultrashort pulsed laser ablation in hard tissue using inline coherent imaging," *Lasers Surgery Med.*, vol. 44, pp. 249–256, Mar. 2012.

[18] Y. Ji, A. W. Grindal, P. J. L. Webster, and J. M. Fraser, "Real-time depth monitoring and control of laser machining through scanning beam delivery system," *J. Phys. D, Appl. Phys.*, vol. 48, p. 155301, Mar. 2015.

[19] S. Donati, "Developing self-mixing interferometry for instrumentation and measurements," *Laser Photon. Rev.*, vol. 6, no. 3, pp. 393–417, May 2012.

[20] F. P. Mezzapesa *et al.*, "High-resolution monitoring of the hole depth during ultrafast laser ablation drilling by diode laser self-mixing interferometry," *Opt. Lett.*, vol. 36, no. 6, pp. 822–824, Mar. 2011.

[21] F. P. Mezzapesa, V. Spagnolo, A. Ancona, and G. Scamarcio, "Detection of ultrafast laser ablation using quantum cascade laser-based sensing," *Appl. Phys. Lett.*, vol. 101, no. 17, p. 171107, Oct. 2012.

[22] F. P. Mezzapesa *et al.*, "Real time ablation rate measurement during high aspect-ratio hole drilling with a 120-ps fiber laser," *Opt. Exp.*, vol. 20, no. 1, pp. 663–671, Jan. 2012.

[23] A. G. Demir, B. Previtali, A. Magnani, A. Pesatori, and M. Norgia, "Application of self-mixing interferometry for depth monitoring in the ablation of TiN coatings," *J. Laser Appl.*, vol. 27, no. S2, p. S28005, Feb. 2015.

[24] U. Zabit, F. Bony, T. Bosch, and A. D. Rakic, "A self-mixing displacement sensor with fringe-loss compensation for harmonic vibrations," *IEEE Photon. Technol. Lett.*, vol. 22, no. 6, pp. 410–412, Mar. 15, 2010.

[25] A. Magnani, A. Pesatori, and M. Norgia, "Real-time self-mixing interferometer for long distances," *IEEE Trans. Instrum. Meas.*, vol. 63, no. 7, pp. 1804–1809, Jul. 2014.

[26] M. Norgia, G. Giuliani, and S. Donati, "Absolute distance measurement with improved accuracy using laser diode self-mixing interferometry in a closed loop," *IEEE Trans. Instrum. Meas.*, vol. 56, no. 5, pp. 1894–1900, Oct. 2007.

[27] A. Magnani, A. Pesatori, and M. Norgia, "Self-mixing vibrometer with real-time digital signal elaboration," *Appl. Opt.*, vol. 51, no. 21, pp. 5318–5325, Jul. 2012.

[28] M. Norgia, A. Pesatori, and L. Rovati, "Low-cost optical flowmeter with analog front-end electronics for blood extracorporeal circulators," *IEEE Trans. Instrum. Meas.*, vol. 59, no. 5, pp. 1233–1239, May 2010.

[29] Ş. K. Özdemir, I. Ohno, and S. Shinohara, "A comparative study for the assessment on blood flow measurement using self-mixing laser speckle interferometer," *IEEE Trans. Instrum. Meas.*, vol. 57, no. 2, pp. 355–363, Feb. 2008.

[30] B. N. Chichkov, C. Momma, S. Nolte, F. von Alvensleben, and A. Tünnermann, "Femtosecond, picosecond and nanosecond laser ablation of solids," *Appl. Phys. A*, vol. 63, no. 2, pp. 109–115, Jul. 1996.

[31] C. Dunsby and P. M. W. French, "Techniques for depth-resolved imaging through turbid media including coherence-gated imaging," *J. Phys. D, Appl. Phys.*, vol. 36, no. 14, pp. R207–R227, Jul. 2003.

[32] U. Zabit, O. D. Bernal, and T. Bosch, "Self-mixing laser sensor for large displacements: Signal recovery in the presence of speckle," *IEEE Sensors J.*, vol. 13, no. 2, pp. 824–831, Feb. 2013.

[33] D. C. Montgomery, *Design and Analysis of Experiments*, 5th ed. New York, NY, USA: Wiley, 2001.

[34] P. J. Herre and U. Barabas, "Mode switching of Fabry–Perot laser diodes," *IEEE J. Quantum Electron.*, vol. 25, no. 8, pp. 1794–1799, Aug. 1989.

[35] W. Schulz, U. Eppelt, and R. Poprawe, "Review on laser drilling I. Fundamentals, modeling, and simulation," *J. Laser Appl.*, vol. 25, no. 1, p. 012006, Feb. 2013.

[36] K. Pangovski *et al.*, "Control of material transport through pulse shape manipulation—A development toward designer pulses," *IEEE J. Sel. Topics Quantum Electron.*, vol. 20, no. 5, Sep. 2014, Art. no. 0901413.

[37] D. Bergström, J. Powell, and A. F. H. Kaplan, "A ray-tracing analysis of the absorption of light by smooth and rough metal surfaces," *J. Appl. Phys.*, vol. 101, no. 11, p. 113504, Jun. 2007.

[38] P. Hariharan, *Basics of Interferometry*, 2nd ed. San Diego, CA, USA: Academic, 2006.

[39] P. E. Ciddor, "Refractive index of air: New equations for the visible and near infrared," *Appl. Opt.*, vol. 35, no. 9, pp. 1566–1573, 1996.

[40] E. R. Peck and B. N. Khanna, "Dispersion of nitrogen," *J. Opt. Soc. Amer.*, vol. 56, no. 8, pp. 1059–1063, 1963.

[41] C. R. Mansfield and E. R. Peck, "Dispersion of helium," *J. Opt. Soc. Amer.*, vol. 59, no. 2, pp. 199–203, 1969.

[42] M. Norgia and C. Svelto, "Novel measurement method for signal recovery in optical vibrometer," *IEEE Trans. Instrum. Meas.*, vol. 57, no. 8, pp. 1703–1707, Aug. 2008.

Ali Gökhan Demir was born in Istanbul, Turkey, in 1985. He received the M.Sc. degree in mechanical engineering and the European Ph.D. degree in mechanical engineering from the Politecnico di Milano, Milan, Italy, in 2009 and 2014, respectively.

He has been an Assistant Professor with the department of Mechanical Engineering, Politecnico di Milano, since 2015. He has authored over 50 papers in international journals and international conference proceedings. His current research interests include laser-based manufacturing processes, mainly laser micromachining, additive manufacturing and process monitoring with the SITEC - Laboratory for Laser Applications.

Dr. Demir is a member of AITeM—Italian Association for Manufacturing Technologies and Photonics21—European Technology Platform.

Paolo Colombo was born in Lecco, Italy, in 1990. He received the M.Sc. degree in mechanical engineering from the Politecnico di Milano, Milan, Italy, in 2015, where he is currently pursuing the Ph.D. degree.

He was involved in laser micromachining and process monitoring during his M.Sc. study. His current research interests include laser-based additive manufacturing of metallic materials employing selective laser melting with the SITEC—Laboratory for Laser Applications.

Michele Norgia (S'99–M'01–SM'09) was born in Omegna, Italy, in 1972. He received the M.S. degree (Hons.) in electronic engineering and the Ph.D. degree in electronics engineering and computer science from the University of Pavia, Pavia, Italy, in 1996 and 2000, respectively.

He joined the Electronic and Information Science Department, Politecnico di Milano, Milan, Italy, in 2006, as an Assistant Professor of Electric and Electronic Measurements. Since 2014, he has been an Associate Professor with the Politecnico di Milano. He has authored over 150 papers in international journals or international conference proceedings. His current research interests include optical and electronic measurements, interferometry, chaos in lasers, optical frequency standards, microelectromechanical sensors, biomedical measurements, and instrumentation.

Dr. Norgia is a member of the Italian Association "Group of Electrical and Electronic Measurements."

Barbara Previtali received the Ph.D. degree in manufacturing and production system from the Politecnico di Milano, Milan, Italy, in 2002.

She was an Associate Professor of Manufacturing and Production Systems with the Department of Mechanical Engineering, Politecnico di Milano, from 2011 to 2016. In 2016, she was appointed as a Full Professor with the Mechanical Engineering Department, Politecnico di Milano, where she teaches with the Faculty of Industrial Engineering and the Faculty of Design. She leads the SITEC—Laboratory for Laser Applications, Politecnico di Milano. She also leads PromozioneL@ser with AITeM, which collects Italian laser users in industry and academia. Her current research interests include modeling, optimization and control of laser processes, with special interest in numerical modeling and experimental approaches of welding, heat treatment, micromachining, and cladding laser processes by innovative laser sources, such as fiber and diode lasers. On these research subjects, she has authored or co-authored over 100 papers in refereed international journals and international conferences and two international patents.

Prof. Previtali is a member of the AITeM—Italian Association for Manufacturing Technologies and of Photonics21—European Technology Platform.